The effects of calcium hydroxide and activator chemistry on alkali-activated metakaolin pastes

Karina M. L. Alventosa[1,2] and Claire E. White[1,2,*]

[1]Department of Civil and Environmental Engineering, Princeton University, Princeton, NJ, 08544, USA

[2]Andlinger Center for Energy and the Environment, Princeton University, Princeton, NJ, 08544, USA

* Corresponding author: Phone: +1 609 258 6263, Fax: +1 609 258 2799, Email: whitece@princeton.edu

Postal address: Department of Civil and Environmental Engineering, Princeton University, Princeton NJ 08544, USA

Abstract:

The impact of calcium hydroxide as an additive in sodium hydroxide- and silicate-activated metakaolin pastes is presented, with a primary aim to ascertain the specific effects of calcium on

the reaction kinetics and phase formation. FTIR and XRD are employed to understand the interaction of calcium hydroxide (10 wt. % replacement of metakaolin) in 1, 5 and 10M NaOH-activated pastes (and equivalent molarity Na_2SiO_3-activated pastes), with a focus on its impact on the nanoscale properties of the sodium-alumino-silicate-hydrate (N-A-S-(H)) gel. *In situ* FTIR and ICC are used to assess the impact of calcium hydroxide on the reaction kinetics, including the rate of metakaolin dissolution and associated rate of N-A-S-(H) gel growth. It is found that calcium hydroxide is effective at accelerating the reaction kinetics of 5M Na_2SiO_3-activated metakaolin due to the formation of an initial calcium-rich gel that promotes additional metakaolin dissolution and enhances N-A-S-(H) gel formation.

Keywords: Alkali-activated materials, metakaolin, calcium addition, amorphous material

1. Introduction

Concrete is an integral component of infrastructure projects (i.e., roads, bridges, buildings, drainage, water and transport) and the most readily available construction material worldwide due to its economic and structural advantages [1]. However, this building material has significant environmental consequences since the production of ordinary Portland cement (OPC), a principle component of concrete, accounts for 5-8% of global anthropogenic CO_2 released into the atmosphere [2]. As mitigation of CO_2 emissions is a prevalent discussion on the global scale, alternative cementitious materials are quickly emerging due to the demands of an ever increasingly industrialized and consumption-oriented society. One type are alkali-activated materials, an established option that has been used in a variety of projects around the globe [3]. In general, the

term ‘alkali-activation’ describes the process where a precursor powder, typically of the aluminosilicate form, is mixed with an alkaline source, the ‘activator’, to form a hard binder product [3]. Previous research on alkali-activated materials for large-scale use focused on the utilization of products made with blast furnace slag (subsequently denoted by slag) and coal-derived fly ash as precursors [4]. These precursors are also regularly used as supplementary cementitious materials (SCMs) in OPC-based concrete. Recently, the availability of slag and fly ash has dwindled. Due to reported decreases in coal consumption, there have been fly ash shortages recorded in 2016, which does not bode well for the increased demands of a growing construction industry [5,6]. The availability of slag is expected to remain volatile due to unpredictable steel production trends and varying country imports [5].

These shortages of fly ash and blast furnace slag have necessitated renewed research of other precursor options for alkali activation such as metakaolin, a calcined form of kaolinitic clay [7,8]. Kaolin is a common clay, accounting for 57% of the 1.66 billion dollars of clay sold by domestic producers in the United States in 2003 [9]. Notably, quantities of kaolin significantly exceed the availability of fly ash and slag [10]. The calcination process of kaolinite, the main mineral phase in kaolin clay, involves heating the mineral to approximately 550 to 750 °C to induce dehydroxylation of the crystalline layered aluminosilicate structure and subsequent formation of an amorphous layered phase [11–13]. The amorphous nature of metakaolin combined with the highly strained alumina sites makes this aluminosilicate quite reactive in high pH environments [14,15]. There are still several significant technical barriers to the use of alkali-activated metakaolin in the construction industry, specifically, the need for caustic activating solutions

[8,16], slow setting times [4,17], and the high-water demand due to high-surface area plate-like particle shapes [16,18].

The alkali activation process of metakaolin can be generally described as a multi-step process in which (i) the precursor dissolves due to its reactivity in the alkaline activating solution, releasing ionic species into solution, (ii) the ionic species (silicate and aluminate monomers) undergo oligomerization via condensation reactions, and (iii) the gel product precipitates via condensation reactions between oligomers, with some systems undergoing an Ostwald ripening process [16,19–21]. The final main binder gel, a sodium-aluminosilicate-hydrate (N-A-S-(H)) gel (analogue K-A-S-(H) gel when potassium is used as the alkali source), is characterized by a three-dimensional aluminosilicate structure with silica as Q^4 units and alumina in q^4, where the negative charge associated with the alumina sites is charge-balanced by the positive alkali ions [22–24]. The main impetus for the use of high concentration activating solutions is the need for adequate dissolution kinetics of metakaolin and ample strength development subsequent to synthesis. The existing literature on alkali-activated metakaolin consistently reports that high molarity alkaline solutions/activators are required for creation of a mechanically-strong binder [16,25,26]. In particular, for low calcium binders, such as metakaolin, the activating solution concentrations exceed 5M (e.g., molarity of a NaOH solution or equivalent alkali concentration for a sodium silicate solution), with some overly excessive concentrations as high as 20M [8,16,26]. Adequate dissolution of NaOH-activated metakaolin has been obtained using 10M to 12M activators, but with 5M, minimal metakaolin dissolution occurs [26,27]. Safety is a priority in the construction industry, and the use of caustic, high pH activating solutions is neither ideal nor practical.

Additional research is required to lower the activator pH without compromising on short- and long-term performance properties.

Previous research focused on accelerating the reaction kinetics and associated short-term performance properties of alkali-activated metakaolin include the addition of calcium hydroxide, gypsum and blast furnace slag as calcium sources [26,28–37], partially due to the relative abundance of calcium-based additives. Given the limited availability of blast furnace slag, and the classification of gypsum as a weak base, calcium hydroxide is the most promising additive to manipulate the alkali activation reaction. The addition of calcium hydroxide to fly ash activated samples (using hydroxide or silicate activation) allows a greater degree of reaction by increasing the amount of reacted fly ash [38,39]. During the initial 24 hours of setting, other previous attempts to augment the reaction kinetics of sodium hydroxide-activated metakaolin with calcium hydroxide were not successful, where the behavior was attributed to the low aqueous silicate concentration and a propensity for the rapidly released aluminate species to quickly react with any recently dissolved silicate species to form a gel on the reacting precursor particles, regardless of whether calcium hydroxide was present or not [34].

A similar system to hydroxide-activated metakaolin where calcium hydroxide is known to have a significant impact is alkaline aluminate solutions (and alkaline silicate solutions). It is known that solid calcium aluminate hydrate phases, such as tricalcium aluminate hexahydrate, readily form when highly alkaline aluminate solutions (such as those with compositions similar to the liquors associated with the Bayer process) are mixed with slaked lime (i.e., calcium hydroxide) at ambient or elevated temperatures, leading to the existence of 6-coord alumina [40,41]. From existing

literature, it is apparent that such a phase does not form when calcium hydroxide (or lime) is added to a hydroxide-activated metakaolin paste [19,26,34]. However, it remains unclear why this is the case from a mechanistic viewpoint. One possible explanation is that even though alumina is preferentially released during the initial stages of metakaolin dissolution, the concentration of aqueous aluminate species is such that there is an insufficient supply of alumina near the calcium hydroxide particles to enable the crystalline calcium aluminate hydrate phase to form [20,42]. On the other hand, the N-A-S-(H) gel does eventually form since the aluminate species that are released due to dissolution are located in the vicinity of the silicate source (i.e., the reacting metakaolin particles). Yet, an *in situ* phase formation study is needed to see if any transient phases, such as calcium aluminate hydrate, are apparent during hydroxide activation of metakaolin with calcium hydroxide.

Contrary to the limited effects of calcium hydroxide in hydroxide-activated metakaolin, recently it has been shown that calcium hydroxide leads to more rapid and extensive precursor dissolution in silicate activation of metakaolin (system stoichiometry of $NaAlSi_2O_6 \cdot 5.5H_2O$), together with faster gel precipitation, and subsequently a faster set time (from Vicat testing), as determined using ^{27}Al nuclear magnetic resonance (NMR) and quantification of alumina sites as a function of reaction time (i.e., amount of 4-, 5- and 6-coord alumina) [34]. Chen *et al.* reported that the silicate-activated metakaolin with additional calcium hydroxide forms an initial calcium-(alumino)-silicate-hydrate (C-(A)-S-H) gel (which also likely contained sodium) due to the interaction of calcium with the free silica from the activator [34]. Yet, setting was not detected by Chen *et al.* until substantial precipitation of the N-A-S-(H) gel was observed. The precipitation of C-(A)-S-H gel was postulated to improve the rate of dissolution and setting by preventing the buildup of a

129 diffusion-limiting N-A-S-(H) gel on the dissolving metakaolin surface, as well as by decreasing
130 the aqueous silicate concentration. Similar behavior has been observed in silicate-, carbonate- and
131 sulfate-activated slag, where calcium-silicate-hydrate (C-S-H), calcium carbonate and calcium
132 sulfate phases are seen to initially form (respectively), followed by slag dissolution and formation
133 of the main sodium-containing calcium-alumino-silicate-hydrate C-(N)-A-S-H gel [43–47].
134
135 Here, the impact of a small amount of calcium hydroxide (10 wt. % replacement of precursor) on
136 the alkali-activated metakaolin reaction is investigated according to activator type (NaOH and
137 Na_2SiO_3) and activator concentration (1, 5 and 10M (moles of NaOH per liter of H_2O, or equivalent
138 Na concentration for Na_2SiO_3 activator)). Isothermal conduction calorimetry (ICC) is used to
139 evaluate the reaction kinetics of the alkali-activated metakaolin pastes and the extent of calcium
140 hydroxide dissolution. Moreover, Fourier transform infrared spectroscopy (FTIR) and X-ray
141 diffraction (XRD) are employed to further understand the interaction of calcium hydroxide in the
142 systems, with a focus on the impact of additional calcium on the nanoscale properties of the N-A-
143 S-(H) gel. For the systems where calcium hydroxide is seen to significantly dissolve, *in situ* FTIR
144 analysis is used to elucidate the mechanism by which calcium is incorporated into the reaction
145 product(s). From these results the efficacy of calcium hydroxide to manipulate the reaction kinetics
146 of alkali-activated metakaolin pastes is discussed. Finally, a brief overview of the impact of
147 calcium hydroxide on the CO_2 emissions of these pastes is provided.
148

2. Materials and Methods

2.1 Materials

This experiment required two types of activating solution: a Na_2SiO_3 solution, and a NaOH solution. The Na_2SiO_3 solution was prepared using PQ Corporation product "D" sodium silicate solution with a SiO_2/Na_2O wt. ratio of 2 and a chemical composition of 14.7 wt. % Na_2O, 29.4 wt. % SiO_2 and 55.9 wt. % H_2O [48]. The PQ D silicate solution was mixed with solid NaOH and deionized water for at least 24 hours prior to activation to achieve the appropriate silicate speciation (for a Na_2SiO_3 solution with the equivalent Na content of 10M NaOH solution: 27.8 wt. % of Na_2O relative to solid precursor, with a SiO_2/Na_2O molar ratio of 1 and a H_2O/precursor wt. ratio of 0.9). The NaOH solution was prepared with solid NaOH pellets (CAS#1310-73-2, Sigma-Aldrich, St. Louis, MO) dissolved in deionized water. The molarities of the activating solutions studied in this investigation were 1, 5 and 10M (relative to molarity of the NaOH activating solution) which equate to 2.78, 13.9 and 27.8 wt. % Na_2O relative to solid precursor, respectively. All samples were synthesized using a H_2O/precursor wt. ratio of 0.9.

Two precursor compositions were studied, specifically (i) metakaolin and (ii) metakaolin with calcium hydroxide. BASF MetaMax was used as the metakaolin source, which is a highly reactive form of metakaolin with a 1.7 wt. % anatase impurity [49] (denoted as 100MK). The second precursor consisted of 90 wt. % MetaMax and 10 wt. % calcium hydroxide (reagent grade, >95%, Sigma Aldrich, St. Louis, MO) combined by vigorous shaking for 15 minutes in 100g batches prior to activation.

Table 1. Sample naming convention.

Short Name	Full Name
1M NaOH + 100MK	100% metakaolin activated with 1M NaOH
5M NaOH + 100MK	100% metakaolin activated with 5M NaOH
10M NaOH + 100MK	100% metakaolin activated with 10M NaOH
1M Na_2SiO_3 + 100MK	100% metakaolin activated with 1M Na_2SiO_3
5M Na_2SiO_3 + 100MK	100% metakaolin activated with 5M Na_2SiO_3
10M Na_2SiO_3 + 100MK	100% metakaolin activated with 10M Na_2SiO_3
1M NaOH + 90MK	90% metakaolin, 10% calcium hydroxide, activated with 1M NaOH
5M NaOH + 90MK	90% metakaolin, 10% calcium hydroxide, activated with 5M NaOH
10M NaOH + 90MK	90% metakaolin, 10% calcium hydroxide, activated with 10M NaOH
1M Na_2SiO_3 + 90MK	90% metakaolin, 10% calcium hydroxide, activated with 1M Na_2SiO_3
5M Na_2SiO_3 + 90MK	90% metakaolin, 10% calcium hydroxide, activated with 5M Na_2SiO_3
10M Na_2SiO_3 + 90MK	90% metakaolin, 10% calcium hydroxide, activated with 10M Na_2SiO_3

To synthesize the pastes, the precursors (100MK and 90MK) were mixed with each type of activating solution in the appropriate proportions for each molarity, creating 12 distinct samples (see Table 1 for naming convention). For each, the precursor and activating solution were manually mixed for one minute, followed by two minutes of vibration mixing at 2500 rpm. The pastes were then sealed in airtight containers and left to solidify in ambient conditions for 7 days prior to XRD and *ex situ* FTIR analysis. The *in situ* FTIR testing involved mixing the samples using the same procedure followed by immediate loading on the attenuated total reflectance (ATR) attachment of the instrument and covering with ParaFilm wax paper to prevent drying of the sample. To maintain constant contact between the sample and the diamond, force was applied on the ATR attachment after 24 hours.

2.2 Experiment Techniques

2.2.1 Gel Formation and Reaction Kinetics

After 7 days of curing, each sample was analyzed with a Perkin Elmer Frontier FT-IR Spectrometer using an ATR attachment (Frontier MIR with a Frontier UATR diamond). The instrument was purged with N_2 gas to eliminate atmospheric H_2O and CO_2 contributions. 32 scans were taken for each sample, with a scan speed of 1 cm/s, a resolution of 4 cm^{-1} and a wavenumber range of 500 to 4000 cm^{-1}. Additionally, the FTIR was used for 7-day continuous testing in which a spectrum consisting of 32 individual scans was recorded every 5 minutes for the first 3 days, and singular measurements were performed at 4, 5, 6 and 7 days.

A TAM Air (TA Instruments) was used to obtain ICC data at 25 °C. For each sample, 5g in total was mixed by hand for 1 minute and by vibration at 2500 rpm for 2 minutes then immediately loaded into a plastic vial and loaded in the calorimeter. 5g of deionized water in a plastic vial was used as the reference sample. All samples were measured in the instrument for 7 days. Data are report in Joules per gram of paste.

2.2.2 Phase characterization

A Bruker D8 Advance diffractometer with a Ag-tube was used to provide mineralogy analysis for each sample. After a curing time of 7 days, the samples were ground into powders using a mortar and pestle, loaded into 1mm polyimide capillary tubes, and sealed with quick set epoxy. The

primary horizontal exit slit of the instrument was set at 1.2mm and the Söller slits on the primary and secondary optics were 2.5°. The secondary horizontal slit was set at 6mm (fully open). The rotation speed of the capillaries was set to 60 rpm and 2θ scans were collected from 3° to 30° using a step size of 0.025° and a count time of 10 sec/step.

3. Results and Discussion

3.1 Neat alkali-activated metakaolin: Structure and Reaction Kinetics

The influence of activator type and concentration on the phase formation in alkali-activated metakaolin are depicted in Figures 1 and 2 (NaOH +100MK and Na_2SiO_3 + 100MK, respectively). This section will discuss metakaolin dissolution and gel formation.

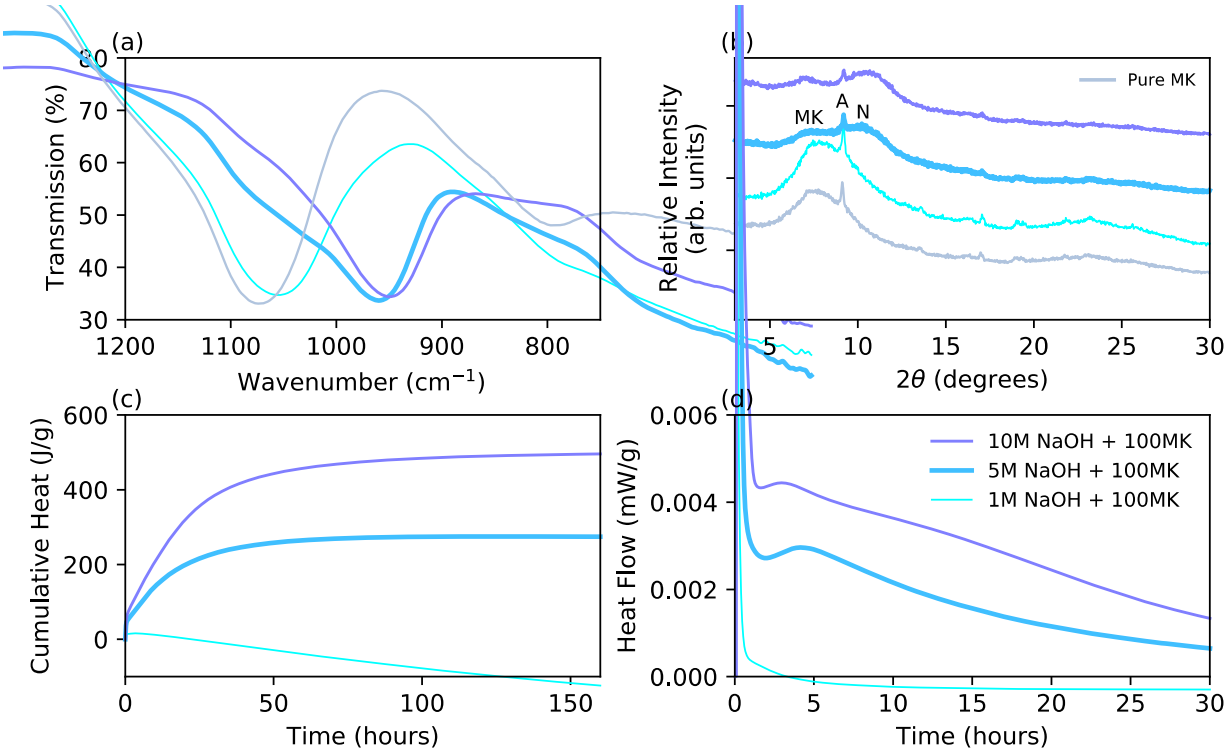

Figure 1. NaOH-activated metakaolin pastes synthesized using 1, 5 and 10M activators. (a) FTIR spectra at 7 days and the spectrum of metakaolin. (b) Stacked XRD patterns at 7 days and the XRD pattern of metakaolin (A = anatase, N = N-A-S-(H) gel, MK = metakaolin). Data obtained using Ag-radiation. (c) Cumulative heat (with respect to grams of metakaolin in original mix) curves up to 7 days. (d) Heat flow curves (with respect to grams of metakaolin in original mix) up to 30 hours.

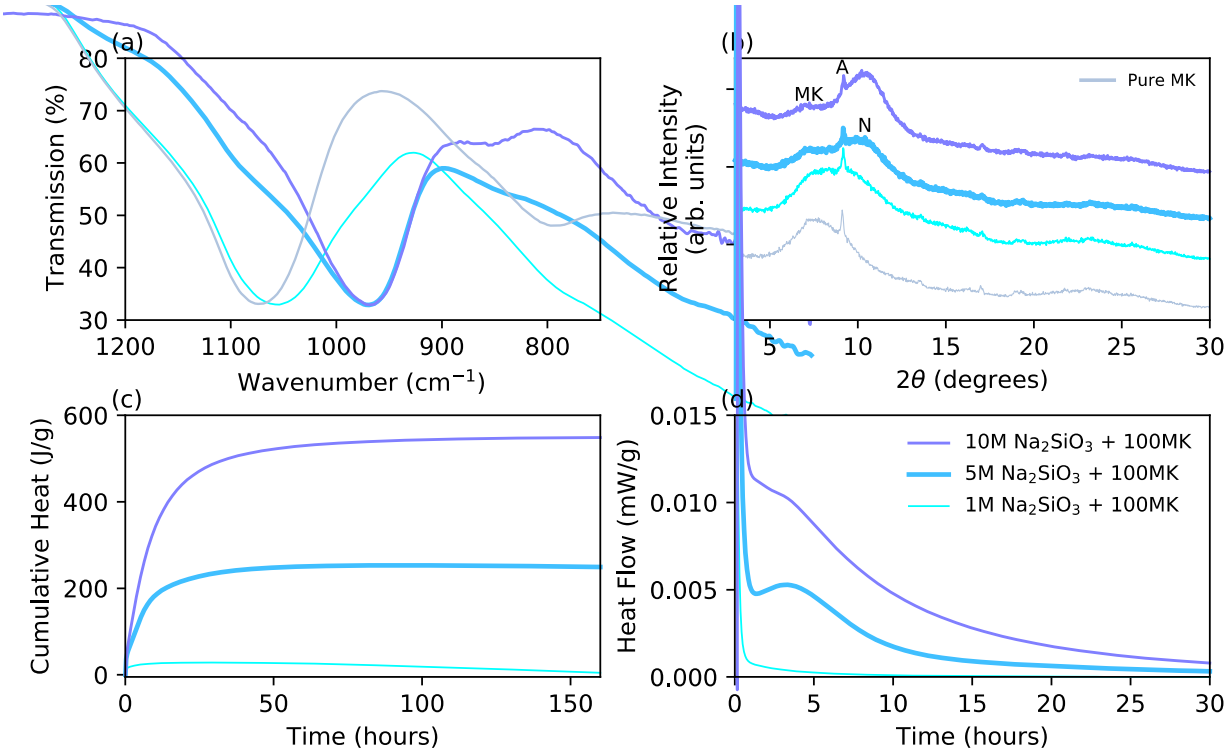

Figure 2. Na_2SiO_3-activated metakaolin pastes synthesized using 1, 5 and 10M activators. (a) FTIR spectra at 7 days and the spectrum of metakaolin. (b) Stacked XRD patterns at 7 days and the XRD pattern of metakaolin (A = anatase, N = N-A-S-(H) gel, MK = metakaolin). Data obtained using Ag-radiation. (c) Cumulative heat (with respect to grams of metakaolin in original mix) curves up to 7 days. (d) Heat flow curves (with respect to grams of metakaolin in original mix) up to 30 hours.

3.1.1 Metakaolin Dissolution and Extent of Gel Formation

It is clear from Figures 1a and 2a that the 1M activators fail to induce sufficient metakaolin dissolution. Notably, the FTIR asymmetric Si-O-T stretching band in these 1M pastes is located at

a similar wavenumber as metakaolin (1074, 1054, 1055 cm^{-1} for metakaolin, 1M NaOH + 100MK, 1M Na_2SiO_3 + 100MK, respectively) [50]. The lack of metakaolin dissolution is also apparent in the XRD patterns of the 1M pastes when compared to those of metakaolin and higher molarity pastes (Figures 1b and 2b). Conversely, Figures 1a and 2a clearly demonstrate that the 5 and 10M pastes have undergone a significant amount of metakaolin dissolution by the shift of the Si-O-T stretching band to 960 and 950 cm^{-1} for 5 and 10M NaOH + 100MK pastes, respectively, and to 970 and 968 cm^{-1} for 5 and 10M Na_2SiO_3 + 100MK pastes, respectively. Metakaolin consists of Q^4(1Al) silicon centers, where each tetrahedral silicon atom is linked to four other silicon/aluminum atoms via bridging oxygens (Q^4), with one of the atoms being aluminum (1Al) [13,51]. As metakaolin dissolves and N-A-S-(H) gel precipitates, the distribution of Si-O-T linkages changes, specifically by the shift from Q^4(1Al) to: (i) predominantly Q^4(4Al) and Q^4(3Al) for 10M NaOH + 100MK and (ii) mainly Q^4(3Al), Q^4(2Al) and Q^4(1Al) for 10M Na_2SiO_3 + 100MK [52]. A lower wavenumber for N-A-S-(H) gel indicates a higher percentage of Si-O-Al linkages, as demonstrated by the 10M NaOH + 100MK [53]. The FTIR spectrum is comprised of contributions from all phases, including unreacted metakaolin and silicate species in the pore solution. Figures 1a and 2a also show that there is more unreacted metakaolin present in the 5M pastes compared with the 10M, specifically by the more prominent shoulder between 1000 and 1100 cm^{-1}.

Analysis of the XRD data provides complementary information to the FTIR findings, where significant changes are visible for the 5 and 10M pastes compared to the 1M (Figures 1b and 2b). The main diffuse XRD peak for the 1M pastes (for both NaOH + 100MK and Na_2SiO_3 + 100MK) is centered at approximately 8 °2θ (Ag-radiation, indicative of metakaolin) that shifts to ~10-11 °2θ for the 5 and 10M pastes due to the formation of N-A-S-(H) gel [17,54–56]. The diffuse peak

attributed to the N-A-S-(H) gel is at a slighter higher 2θ value for the 10M pastes than the 5M pastes (Figures 1b and 2b), consistent with the slight differences seen in the FTIR wavenumbers discussed above (10M pastes correlate to lower wavenumbers than the 5M pastes). Hence, it is clear that a substantial amount of metakaolin dissolution has occurred in the 10M pastes (both NaOH + 100MK and Na_2SiO_3 + 100MK), compared with a sizable amount in the 5M pastes and minimal dissolution in the 1M pastes, as anticipated [50].

The extent of gel formation is expected to directly correlate with the extent of metakaolin dissolution, and therefore, based on the above discussion, the 5M pastes will form less gel than the 10M. This is confirmed by the isothermal calorimetry data (Figures 1c and 2c), where the cumulative heat of the 5M NaOH + 100MK paste, with respect to the amount of metakaolin in the sample, reaches a plateau at 272 J/g, while the corresponding data for the 10M NaOH + 100MK paste reaches 475 J/g (Figure 1c). A similar trend is visible for the Na_2SiO_3 + 100MK pastes in Figure 2c (249 J/g for 5M paste versus 548 J/g for 10M). Although it is difficult to decipher from ICC data whether metakaolin dissolution, gel formation, or both are affected by a reduction in activator alkalinity, these data sets in conjunction with analysis of the FTIR and XRD data reveal some important qualitative trends. Specifically, from the FTIR data, it is clear that a higher amount of unreacted metakaolin remains in the 5M pastes compared with the 10M pastes (shoulder between 1000 and 1100 cm^{-1}), and therefore the increase in the cumulative heat from 5 to 10M is partially associated with additional metakaolin dissolution. Nevertheless, the prominent gel peak for 10M Na_2SiO_3 + 100MK metakaolin in Figure 2b (XRD data) compared with its 5M counterpart shows that there is additional gel formation in this paste, which will also contribute to the increase in cumulative heat in Figure 2c.

Identification of the dissolution-dominated and gel precipitation-dominated regions of the ICC data is common in the literature [57]. For OPC, there is a well-defined induction period in the heat flow curve between these two regions [58], which is manifested as a prolonged minimum in this curve. However, it is clear from Figures 1d and 2d that no such induction period exists in alkali-activated metakaolin. Furthermore, as is the case for OPC-based systems, the initial peak that overlaps with sample mixing and/or instrument loading is attributed to dissolution dominated processes [27,44]. Contrary to this common explanation, Gong *et al.* showed that this initial peak seen in an ICC heat flow curve (at ~10 min) of alkali-activated slag can be solely attributed to heat from particle wetting (same heat flow profile obtained for an alkali-activated slag and a slag-water mixture), and therefore dissolution processes do not contribute to heat flow (in alkali-activated systems) in this region (up to ~10-15 minutes after mixing) [43]. Furthermore, Gong *et al.* reported a similar heat flow region associated with metakaolin wetting, where the heat flow curve reached a maximum of ~34mW/g at ~5 minutes in a metakaolin-water system [43]. It is clear that the initial peak in the heat flow curve of alkali-activated systems (prior to ~15 min) is mainly due to heat release due to particle wetting, and not, in contrast to the existing literature, dissolution processes.

Taking into consideration the above discussion on the dominance of particle wetting before ~10-15 minutes, the increase in cumulative heat that occurs over the course of hours in Figures 1c and 2c (up to ~50 hours) must be attributed to both metakaolin dissolution and gel precipitation. It has been reported in the past that dissolution of metakaolin contributes a heat release of ~1200 J/g (value obtained from ref. [59]). Evidently, this value is more than double the cumulative heat of

300 the 10M pastes, despite neglecting the impact of partial metakaolin dissolution, other exothermic
301 reactions (such as gel formation) and endothermic contributions. Nevertheless, it does
302 demonstrate that the heat release associated with metakaolin dissolution is a significant contributor
303 to the cumulative heat curves seen in Figures 1c and 2c.

304

305 ***3.2 Neat alkali-activated metakaolin: Structural Evolution***

306 To obtain reaction kinetics data complementary to the ICC, *in situ* ATR-FTIR has been employed
307 where the asymmetric Si-O-T stretching band of the alkali-activated metakaolin pastes has been
308 recorded as a function of reaction time (Figure 3, converted to absorption to aid visual analysis).
309 From these data (also given as false color plots in the Supplemental Material (Figures S2 and S3))
310 the location of the minimum transmission value for this mode is tracked as a function of time in
311 Figure 4. For 10M NaOH + 100MK, the intensity of the main Si-O-T band associated with N-A-
312 S-(H) gel appears after approximately 5 hours and is centered around 950 cm^{-1}, as shown in Figure
313 4. Prior to 5 hours, metakaolin contributions dominate the main Si-O-T band at around 1060 cm^{-1}.
314 Conversely, it is evident that the intensity in the 10M Na_2SiO_3 + 100MK paste is around 950-
315 970 cm^{-1} for the duration of the *in situ* experiment (Figure 4). Contrary to these 10M NaOH +
316 100MK findings, there is no initial peak in 10M Na_2SiO_3 + 100MK with a wavenumber similar to
317 metakaolin. Instead, as seen in Figure 4, the main Si-O-T peak is positioned at 972 cm^{-1} from the
318 outset (~15 minutes after mixing) and undergoes a slight shift to ~950 cm^{-1} after 10 hours of
319 reaction and to ~948 cm^{-1} by 30 hours. The FTIR spectrum of a Na_2SiO_3 solution with similar
320 composition (Si/Na molar ratio of 0.5, H_2O wt. % of 55.3) to the 10M Na_2SiO_3 activating solution
321 (Si/Na molar ratio of 0.5, H_2O wt. % of 62.2) consists of a Si-O-Si band at 967 cm^{-1} [60], where

additional data from ref. [61] gives the band at ~975 cm^{-1} for a sodium silicate solution with a Si/Na molar ratio of 0.5 but with an unknown H_2O/Na_2O molar ratio. Therefore, contributions from the initial silicate activator will skew the main Si-O-T band to lower wavenumbers (compared with pure metakaolin) from the outset.

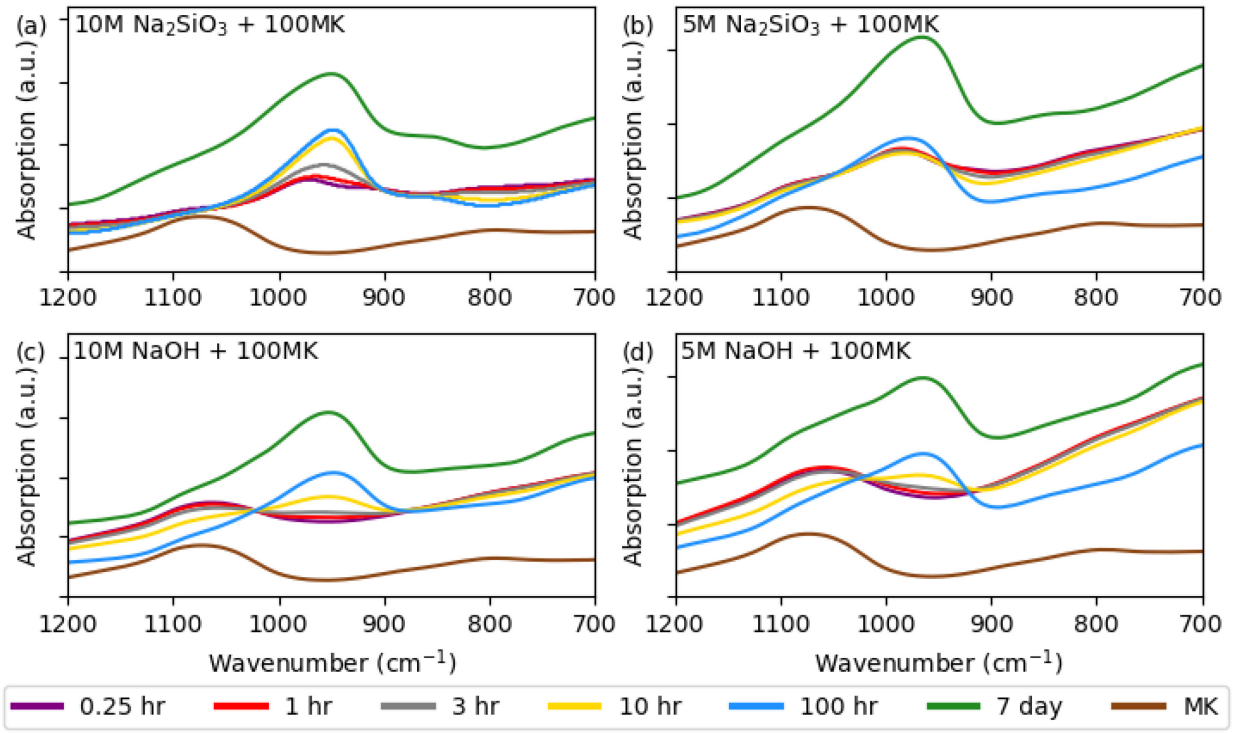

Figure 3: Select FTIR spectra of (a) 10M Na_2SiO_3 + 100MK (b) 5M Na_2SiO_3 + 100MK, (c) 10M NaOH + 100MK, and (d) 5M NaOH + 100MK, extracted from the *in situ* FTIR data (represented as false color plots in Supplementary Material (Figures S2 and S3)), converted from transmission to absorption to aid data analysis. The metakaolin and 7 day data are vertically offset with respect to the *in situ* data.

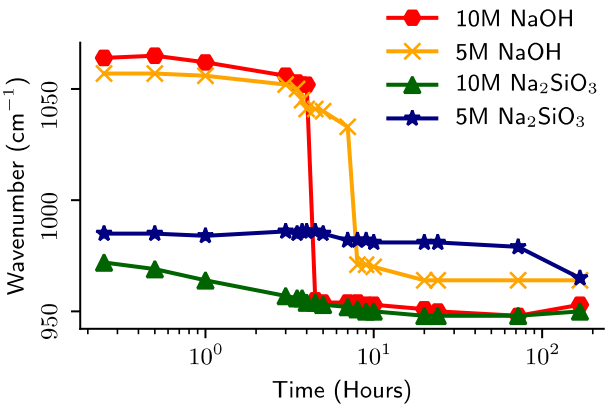

Figure 4: Wavenumber position of main FTIR asymmetric Si-O-T stretching band during the initial 168 hours of alkali activation for 5M and 10M NaOH + 100MK and 5M and 10M Na_2SiO_3 + 100MK.

Similar trends occur in the 5M pastes, a singular difference that, for 5 and 10M NaOH + 100MK pastes, the 5M paste undergoes significant gel formation after ~8 hours instead of at 5 hours for the 10M paste (Figure 4). The elongated dissolution period for the 5 and 10M NaOH + 100MK pastes (prior to the start of substantial gel formation) may explain why this system (e.g., 10M NaOH + 100MK) achieves a higher extent of metakaolin dissolution (i.e., less residual metakaolin at later age) compared with the 10M Na_2SiO_3 + 100MK system. These findings, specifically, the dissolution dominated region up to ~5-8 hours in the 5 and 10M NaOH + 100MK systems, are in general agreement with previous data from X-ray pair distribution function (PDF) analysis [21] and small-angle scattering (SAS) [62]. Specifically, PDF and SAS data revealed that the silicate-activated metakaolin switches from dissolution dominated to gel formation at ~4 hours, contrasting with the longer dissolution-dominated region for hydroxide-activated (PDF data show dissolution continues past 10 hours of reaction). There are some interesting changes between 100 hours and 7

days in terms of the position of the Si-O-T vibrational mode, with the most significant change seen for 10M Na_2SiO_3 + 100MK which transitions from ~950 to 968 cm^{-1} (10M NaOH + 100MK shifts from ~953 to 950 cm^{-1}, 5M NaOH + 100MK from ~965 to 960 cm^{-1}, and 5M Na_2SiO_3 + 100MK from ~965 to 970 cm^{-1}).

3.3 Impact of calcium hydroxide: Structure and Reaction Kinetics

3.3.1 Calcium hydroxide dissolution

The impact of calcium hydroxide on the reaction kinetics and phase formation in alkali-activated metakaolin is depicted in Figures 5 and 6. From the XRD results (Figures 5b and 6b) it is clear that the calcium hydroxide does not readily dissolve in the 5 and 10M NaOH + 90MK pastes, as demonstrated by the visibility of prominent Bragg peaks attributed to this phase (i.e., portlandite crystal structure). As reported previously in the literature, due to the common ion effect and the high pH environments in the 5M and 10M NaOH systems, the calcium hydroxide is relatively inert and does not participate extensively in gel formation [63]. This is in contrast to the complete dissolution of calcium hydroxide in all Na_2SiO_3-activated pastes, as seen in Figure 6b. The calcium hydroxide in the 1M NaOH + 90MK paste does react to a certain extent, as seen by the reduced intensity of the portlandite Bragg peaks in the XRD data for this sample compared with the 5 and 10M equivalents (Figure 5b), and the shift of diffuse scattering to higher 2θ values (sizable amount of scattering at ~11°) compared with the 1M NaOH + 100MK (at ~8°, similar to metakaolin, see Figure 1b). Furthermore, two hydrate phases are seen to form in 1M NaOH + 90MK: C-S-H gel and stratlingite, as observed previously in the literature for lime-metakaolin pastes [64], although the presence of a small amount of a calcium aluminate hydrate phase cannot be discounted in place of C-S-H gel.

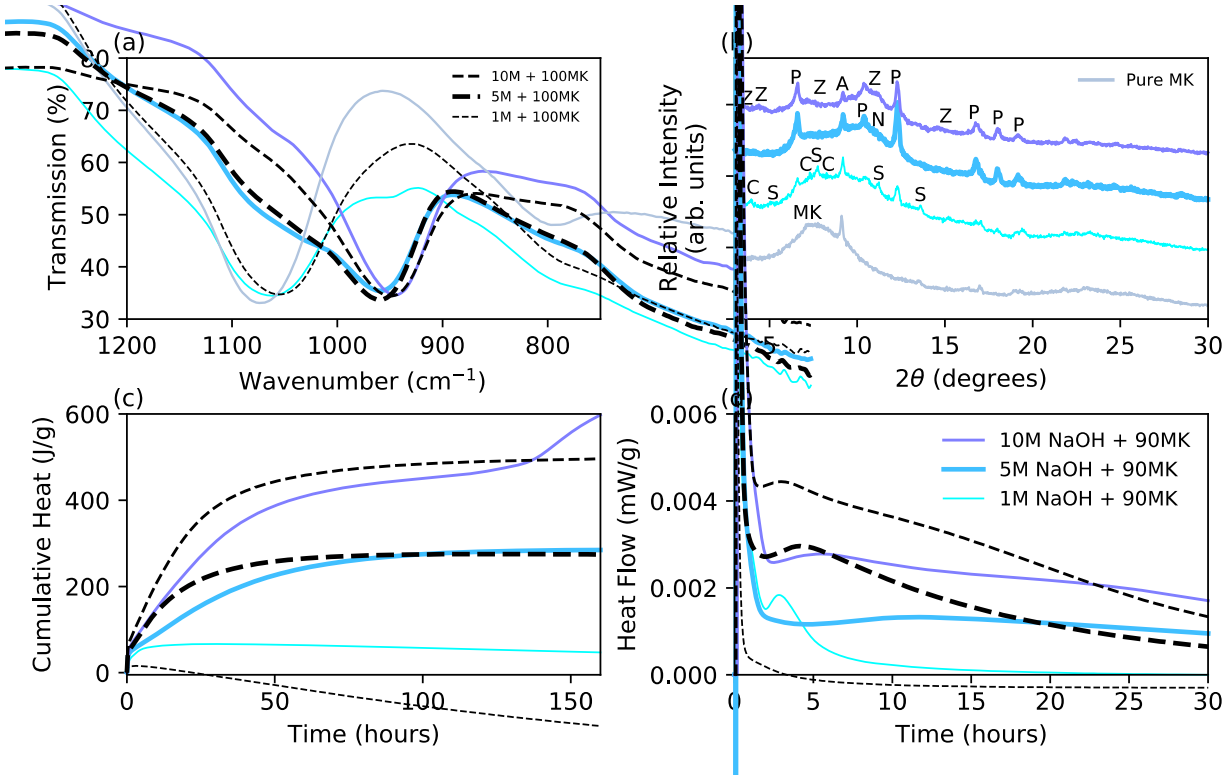

Figure 5: NaOH-activated metakaolin pastes synthesized using 1, 5 and 10M activators and calcium hydroxide (90MK). (a) FTIR spectra at 7 days along with the spectrum of metakaolin. (b) Stacked XRD patterns at 7 days together with the pattern for metakaolin (A = anatase, C = C-S-H gel, N = N-A-S-(H) gel, P = portlandite, S = stratlingite, MK = metakaolin, Z = zeolite A). Data obtained using Ag-radiation. (c) Cumulative heat (with respect to grams of metakaolin in original mix) curves up to 7 days. (d) Heat flow curves (with respect to grams of metakaolin in original mix) up to 30 hours.

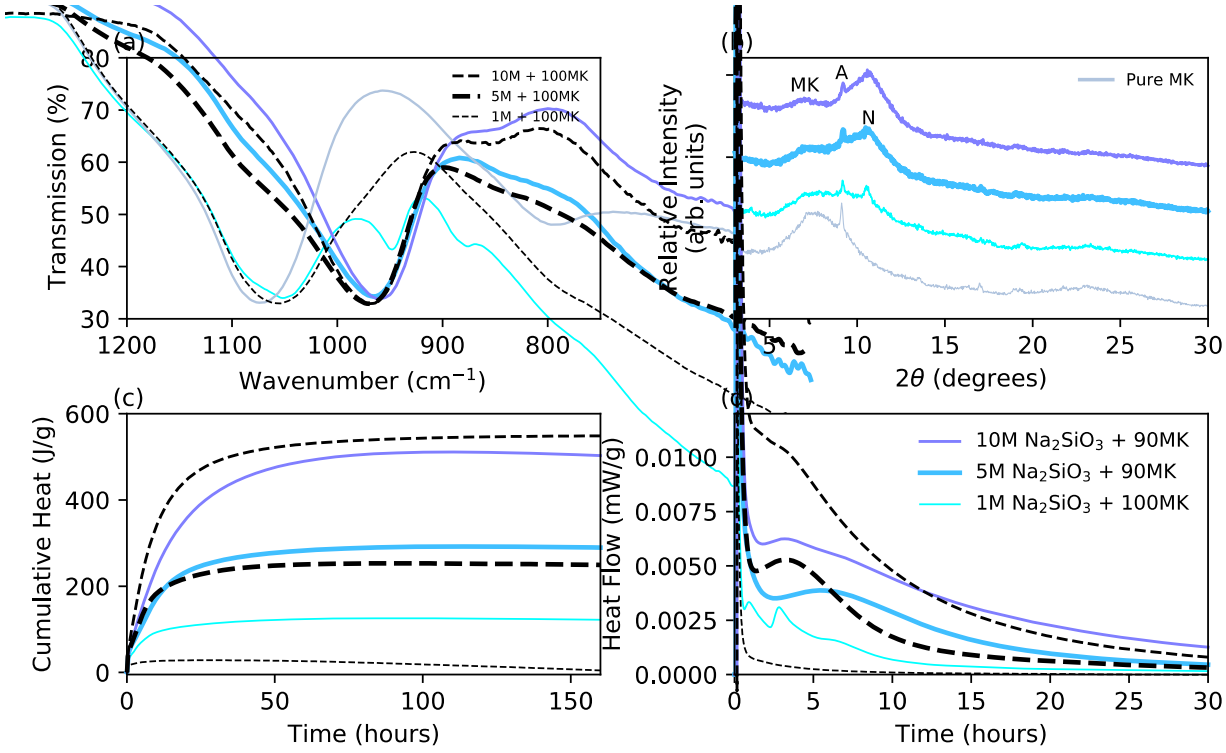

382

383 Figure 6. Na_2SiO_3-activated metakaolin pastes synthesized using 1, 5 and 10M activators and
384 calcium hydroxide (90MK). (a) FTIR spectra at 7 days along with the spectrum of metakaolin. (b)
385 Stacked XRD patterns at 7 days together with the pattern for metakaolin (A = anatase, N = N-A-
386 S-(H) gel, MK = metakaolin). Data obtained using Ag-radiation. (c) Cumulative heat (with respect
387 to grams of metakaolin in original mix) curves up to 7 days. (d) Heat flow curves (with respect to
388 grams of metakaolin in original mix) up to 30 hours.

389

390 *3.3.2 Metakaolin Dissolution and Extent of Gel Formation*

391 Although calcium hydroxide is seen to have minimal impact on the amount of metakaolin
392 dissolved in 5 and 10M NaOH pastes at 7 days (see Figure 5a between 1000 and 1100 cm^{-1} where
393 metakaolin contributions are found), there is a distinct effect on the 5 and 10M Na_2SiO_3 pastes,

where the addition of calcium hydroxide is seen to reduce the intensity of the shoulder attributed to metakaolin indicating that calcium hydroxide may enhance the extent of metakaolin dissolution at 7 days (see 5 and 10M Na_2SiO_3-activated pastes (100MK and 90MK) at 7 days, Figure 6a). For the 1M pastes, it is difficult to ascertain if calcium hydroxide promotes metakaolin dissolution (both for the NaOH- and Na_2SiO_3-activated pastes), however, it is clear that calcium hydroxide impacts gel formation in these systems, demonstrated by the emergence of a small, but evident vibrational mode at ~950 cm^{-1} in both pastes (1M NaOH + 90MK and 1M Na_2SiO_3 + 90MK). This band is attributed to a limited extent of a pozzolanic reaction that forms C-A-S-H gel. Similar gels form initially in silicate-activated Ca-rich precursor systems, for instance silicate-activated slag, where Ca from slag dissolution reacts with silicate species to form C-A-S-H gel followed by additional slag dissolution and formation of the main C-(N)-A-S-H gel [43]. Lastly, there are slight differences in the location of the main Si-O-T band for the 1M 90MK pastes, where calcium hydroxide causes a shift from 1054 to 1062 cm^{-1} in the 1M NaOH + 90MK paste and from 1055 to 1052 cm^{-1} in the 1M Na_2SiO_3 + 90MK paste.

In terms of gel formation and the impact of calcium hydroxide in the 5 and 10M NaOH pastes, the FTIR data in Figure 5a shows that the addition of calcium hydroxide has a minimal impact on the peak location of the Si-O-T vibrational mode for the NaOH-activated pastes (comparing 100MK and 90MK). The only noticeable difference is a slight shift of the Si-O-T band in the 10M NaOH system from 950 to 945 cm^{-1} due to the addition of calcium hydroxide (comparing 100MK and 90MK), but the 5M paste remains at 960 cm^{-1}. The cumulative heat per mass of metakaolin decreases due to the addition of calcium hydroxide in the 10M NaOH paste (prior to zeolite crystallization), specifically from ~480 J/g for 10M NaOH + 100MK to ~435 J/g for 10M NaOH

+ 90MK at 100 hours after mixing. On the other hand, the 5M NaOH pastes (100MK and 90MK) are seen to reach similar values of cumulative heat by 7 days (~273 J/g). For both the 5 and 10M NaOH pastes calcium hydroxide is seen to delay the main rise in cumulative heat (Figure 5c , comparing 100MK and 90MK), indicating that the addition of calcium hydroxide to these pastes leads to an overall slowing down of reaction kinetics during the initial 2-3 days after mixing. Lastly, the inclusion of calcium hydroxide is seen to promote the formation of zeolites at ~140 hours after mixing in the 10M NaOH paste (see 10M NaOH + 90MK ICC data in Figure 5c), where the cumulative heat increases to 596 J/g at 7 days [27] and small Bragg peaks attributed to zeolite A are visible in the XRD data (Figure 5b). A similar cumulative heat increase was seen to occur in the 10M NaOH + 100MK paste at ~220 hours (at ~9 days in the ICC curve, beyond the time scale shown in Figures 1c and 5c).

Calcium hydroxide has a greater impact on phase formation in Na_2SiO_3-activated metakaolin pastes. The asymmetric Si-O-T stretching band shifts to lower wavenumbers when calcium hydroxide is incorporated in these pastes, specifically from 1055 to 1051 cm^{-1} for 1M Na_2SiO_3 + 90MK, 970 to 964 cm^{-1} for 5M Na_2SiO_3 + 90MK, and 967 to 961 cm^{-1} for 10M Na_2SiO_3 + 90MK paste. This indicates a more Ca-rich gel, compared to those without calcium, particularly for the 5 and 10M Na_2SiO_3 + 90MK pastes. Calcium is known to lower the wavenumber of silicate-rich gels; for synthetic C-S-H gels the Si-O-T band is located between 945 cm^{-1} and 955 cm^{-1} [65,66], while for Ca-rich alkali-activated materials (such as slag-based systems) the Si-O-T stretching band is located at 953 cm^{-1} [67] for a 40-day-old hydroxide-activated slag (Na_2O wt. % of 4.0), and the band associated with the equivalent silicate-activated slag (SiO_2/Na_2O molar ratio of 1 for the activator) is found at 941 cm^{-1}. It is important to be cognizant that the uptake of alumina into

the gel will also result in a lowering of the wavenumber, and therefore contributions from this mechanism (alumina uptake) cannot be discounted from the current study.

As mentioned earlier, calcium hydroxide may promote more extensive metakaolin dissolution at 7 days in the Na_2SiO_3-activated pastes (as seen in the FTIR data in Figure 6a via comparison of 5 and 10M Na_2SiO_3 + 100MK with 5 and 10M Na_2SiO_3 + 90MK), however, the ICC data in Figure 6c show that the addition of calcium causes a decrease in cumulative heat for the 10M paste at 7 days (from 548 J/gfor 10M Na_2SiO_3 + 100MK to 500 J/g for 10M Na_2SiO_3 + 90MK), similar to the NaOH-activated pastes. On the other hand, the 5M Na_2SiO_3 + 90MK paste is seen to experience an increase in cumulative heat compared with the 5M Na_2SiO_3 + 100MK paste, 249 J/g, to 285 J/g due to the addition of calcium hydroxide. These observations indicate that the effectiveness of calcium hydroxide to promote metakaolin dissolution and subsequent gel formation is likely dependent on the initial concentration of the Na_2SiO_3 activator, as will be discussed in more detail in Section 3.4. The type of gel that precipitates is unlikely to affect the cumulative heat, since the enthalpy of formation for a C-(N)-A-S-H gel (heat released) has been reported as ranging from 2491 to 2831 kJ/mol (from thermodynamic modeling input data [68] for solid-solution compositions ranging from $(CaO)_{1.25}(Al_2O_3)_{0.125}(SiO_2)_1(H_2O)_{1.625}$ to $(CaO)_1(SiO_2)_{1.5}(H_2O)_{2.5}$), and the enthalpy of formation for N-A-S-(H) gel has been reported as 2642 kJ/mol for a composition of $NaAlSiO_4 \cdot 2.25H_2O$ (2738 kJ/mol for the crystalline version, specifically zeolite A) [69]. Therefore, it is likely that calcium hydroxide is enhancing metakaolin dissolution and associated gel formation in the 5M Na_2SiO_3-activated metakaolin paste.

462 The XRD data also provide important insight on the impact of calcium hydroxide on the gel
463 formation in the 5 and 10M Na_2SiO_3-activated metakaolin pastes. As seen in Figure 6b, calcium
464 influences the shape of the main XRD peak associated with N-A-S-(H) gel. This peak in the 10M
465 Na_2SiO_3 + 90MK paste is more defined than the 100MK counterpart (comparing Figures 2b and
466 Figure 6b), indicating a more ordered gel. Previous research has shown that C-(N)-A-S-H gel
467 formed in silicate-activated slag paste is predominately amorphous, with nanoscale ordering out
468 to ~2.5 nm in the X-ray pair distribution function [70]. Furthermore, N-A-S-(H) gel is entirely
469 amorphous, containing atom-atom correlations only out to ~0.8 nm [28]. This increase in nanoscale
470 ordering of the gel(s) as calcium is added to silicate-activated metakaolin is likely attributed to the
471 formation of the C-A-S-H gel in conjunction with the main N-A-S-(H) gel. Additional research is
472 required to determine the spatial distribution of the C-A-S-H gel in the paste, specifically if two
473 distinct gel regions are present or if calcium is homogeneously distributed throughout the gel
474 phase. Previous research has pointed toward the existence of two distinct gels in silicate-activated
475 metakaolin containing calcium hydroxide during the early stages of reaction [34,66,71,72].
476 Specifically, Chen *et al.* reported that the calcium from calcium hydroxide is initially incorporated
477 into a C-(N)-A-S-H gel (consisting of Q^1, Q^2, Q^3 and Q^4 silicon centers) which exists along with
478 the N-A-S-(H) gel [34]. At later age, the C-A-S-H gel is seen to disappear while a Ca-modified
479 geopolymer gel (i.e., N-(C)-A-S-(H)) forms, consisting of a three-dimensional N-A-S-(H) gel
480 containing calcium ions (i.e., predominately Q^3 and Q^4 silicon centers).

481

482

3.4 Impact of calcium hydroxide: Kinetics

The addition of calcium significantly affects the structural evolution of the gel for both the NaOH- and Na_2SiO_3-activated pastes, as verified by the *in situ* FTIR results (Figures 7 and 8). For the NaOH-activated systems, the addition of calcium hydroxide is seen to delay the emergence of the N-A-S-(H) gel peak (positioned between ~950 and 970 cm^{-1} in Figure 8) by ~3 hours for the 10M system and ~60 hours for the 5M system. On the other hand, for Na_2SiO_3-activated metakaolin, calcium is seen to have an accelerating effect on gel formation, specifically in the 5M system (limited impact on the 10M system). In particular, without calcium hydroxide (Figure 4), the 5M Na_2SiO_3 + 100MK paste is seen to have limited change in the position of the main Si-O-T vibrational mode until ~100 hours at which point the position changes from ~980 to ~965 cm^{-1}, whereas for 5M Na_2SiO_3 + 90MK (Figure 8), there is a gradual change in the wavenumber from the outset of the reaction (i.e., starting within 30 minutes after mixing) until ~70 hours.

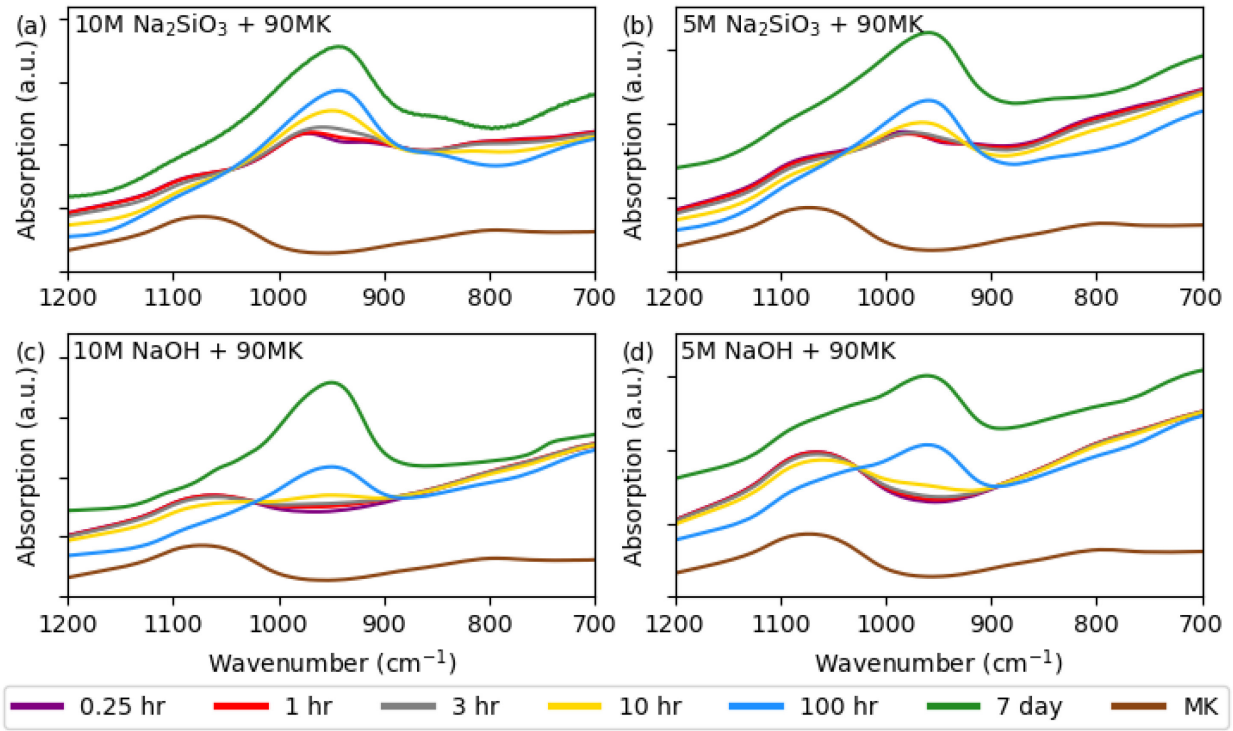

Figure 7: Select FTIR spectra of calcium hydroxide-containing (a) 10M Na_2SiO_3-activated + 90MK (b) 5M Na_2SiO_3 + 90MK, (c) 10M NaOH + 90MK, and (d) 5M NaOH + 90MK, extracted from the false color plots in Supplementary Material (Figures S5 and S6), converted from transmission to absorption to aid data analysis. The metakaolin and 7 day data are vertically offset with respect to the *in situ* data.

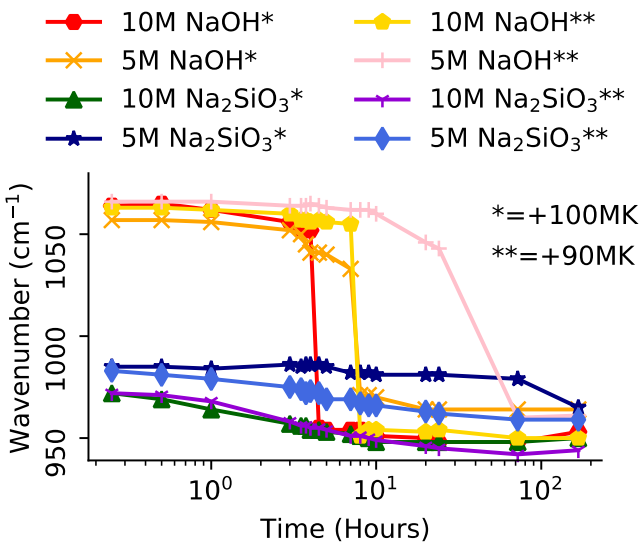

Figure 8: Wavenumber position of main FTIR asymmetric Si-O-T stretching band during the initial 168 hours of alkali activation for 5 and 10M NaOH + 100MK, 5 and 10M NaOH + 90MK, and 5 and 10M Na_2SiO_3 + 100MK, and 5 and 10M Na_2SiO_3 + 90MK.

This gradual change in wavenumber for 5M Na_2SiO_3 + 90MK is indicative of the calcium from calcium hydroxide reacting with the silicate species in solution to form an initial C-A-S-H gel. In fact, careful analysis of the FTIR data sets in Figure 9, which cover the initial 3 hours, reveals that

510 there is initially a small but distinct peak present at ~925 cm^{-1} that is enveloped by the increase of
511 the main peak by 1 hour in both the 5M and 10M Na_2SiO_3 + 90MK pastes. This small peak is not
512 as readily apparent in the 5M and 10M Na_2SiO_3 + 100MK pastes at 15 minutes after mixing (Figure
513 9), indicating that this peak is associated with a calcium-containing phase. Comparison of the peak
514 location (~925 cm-^{1}) with literature data reveals that this peak is likely associated with the Q^2
515 asymmetric Si-O-Si stretching mode (usually located between ~950 and ~970 cm^{-1} for synthetic
516 C-S-H-type gels) [65,73], but with a sizable alumina incorporated into the gel (i.e., C-A-S-H gel),
517 which is known to cause a decrease of the wavenumber [74].

518

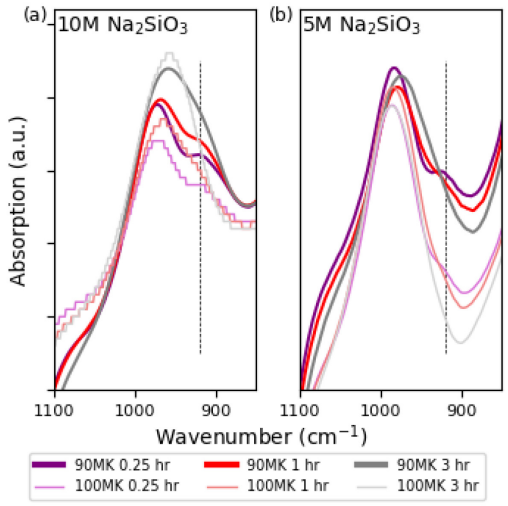

519

520 Figure 9: Early age FTIR spectra of (a) 10M Na_2SiO_3 + 100MK and 10M Na_2SiO_3 + 90MK, and
521 (b) 5M Na_2SiO_3 + 100MK and 5M Na_2SiO_3 + 90MK, extracted from the false color plots in
522 Supplementary Material (Figures S2, S3, S5 and S6) and converted from transmission to
523 absorption to aid data analysis. Although the 10M Na_2SiO_3 + 100MK data sets are relatively coarse
524 this does not affect the conclusions drawn from analysis of these data.

In addition to this C-A-S-H gel peak, the FTIR data reveal that more metakaolin dissolution is occurring in the 5M Na_2SiO_3 + 90MK compared with its 100MK counterpart (see Figure 10). These data in Figure 10 have been obtained by quantification of the FTIR spectra, specifically the amount of unreacted metakaolin relative to the entire paste contributions over a wavenumber range of 880 to 1300 cm^{-1}. The quantification has been carried out using Gaussian peak fitting and a least-squares refinement (implemented in the Fityk software) [75], where first the neat metakaolin FTIR data set was used to obtain the specific Gaussian contributions for subsequent refinement of the unreacted metakaolin component. Second, for the paste at a given age a single scale factor for these metakaolin contributions was refined along with contributions (modeled as Gaussians) from the gel (C-A-S-H and N-(C)-A-S-(H)) and solution. Note that two to four Gaussians were needed for the gel/solution contributions depending on the sample age and composition. The relative area obtained from the Gaussians gave a fractional value for the relative amount of unreacted metakaolin. Prior to this curve fitting procedure, a spline background was refined and subtracted from the FTIR data sets. For the 5 and 10M Na_2SiO_3 + 100MK pastes, along with the 5 and 10M Na_2SiO_3 + 90MK pastes, it was found that the relative amount of metakaolin varied over time from 0.40-0.57 at 5 minutes after mixing to 0.00-0.22 after 7 days. It is known that there is unreacted metakaolin present in similar pastes at 7 days, and therefore the final amounts obtained from FTIR at 7 days (0.00-0.22) are unrealistically low [76]. This necessitated the use XRD data (from Figures 2b and 6b) to determine the final amount of unreacted metakaolin. After background subtraction, four Gaussians were refined against the neat metakaolin XRD data (using least-squares refinement and Fityk) and the overall scale factor associated with the fitted curve was set at 1.0. For each paste, the metakaolin fitted curve and one to two additional Gaussians (used to represent the gel)

548 were refined against the XRD data. The resulting scale factors associated with the unreacted
549 metakaolin contributions were used as the 7 day values for the FTIR fractional amounts.
550 Specifically, rescaling of the FTIR-derived unreacted metakaolin fractional amounts was carried
551 out using the 7 day XRD values as the end point, and 1.0 and 0.9 for the start point (5 minutes after
552 mixing) for the 100MK pastes and the 90MK pastes, respectively.

553

554 Figure 10 shows that the relative amount of unreacted metakaolin in the 5M Na_2SiO_3 + 100MK
555 paste decreases from 1.0 to ~0.9 during the first hour while for 5M Na_2SiO_3 + 90MK the amount
556 of metakaolin remains constant at 0.9. However, following the initial first hour, metakaolin
557 dissolution in the 90MK paste occurs at a faster rate than in the 100MK paste, as demonstrated by
558 the steeper slope seen in Figure 10 (-0.234 for 90MK compared with -0.202 for 100MK). At 7
559 days (176 hours) the 5M Na_2SiO_3 + 90MK paste is seen to have undergone more extensive
560 metakaolin dissolution compared with the 5M Na_2SiO_3 + 100MK paste. Interestingly, comparison
561 of the ICC data in Figure 6c and 6d with Figure 10 shows that the main period of metakaolin
562 dissolution (from ~3 hours onwards) identified in Figure 10 does not coincide with the location of
563 maximum heat flow curve in Figure 6d for the 5M pastes. For 5M Na_2SiO_3 + 100MK paste the
564 heat flow maximum is located at ~3 hours but only approximately 15% of metakaolin has reacted
565 (compared to 45% at 7 days). Similarly, the maximum in the heat flow for the 5M Na_2SiO_3 +
566 90MK paste is located at ~7 hours at which stage only approximately 13% of the original
567 metakaolin in the 90MK paste has reacted (compared to 50% at 7 days). This shows that the rate
568 of metakaolin dissolution cannot be directly assessed from ICC heat flow curves for alkali-
569 activated metakaolin pastes.

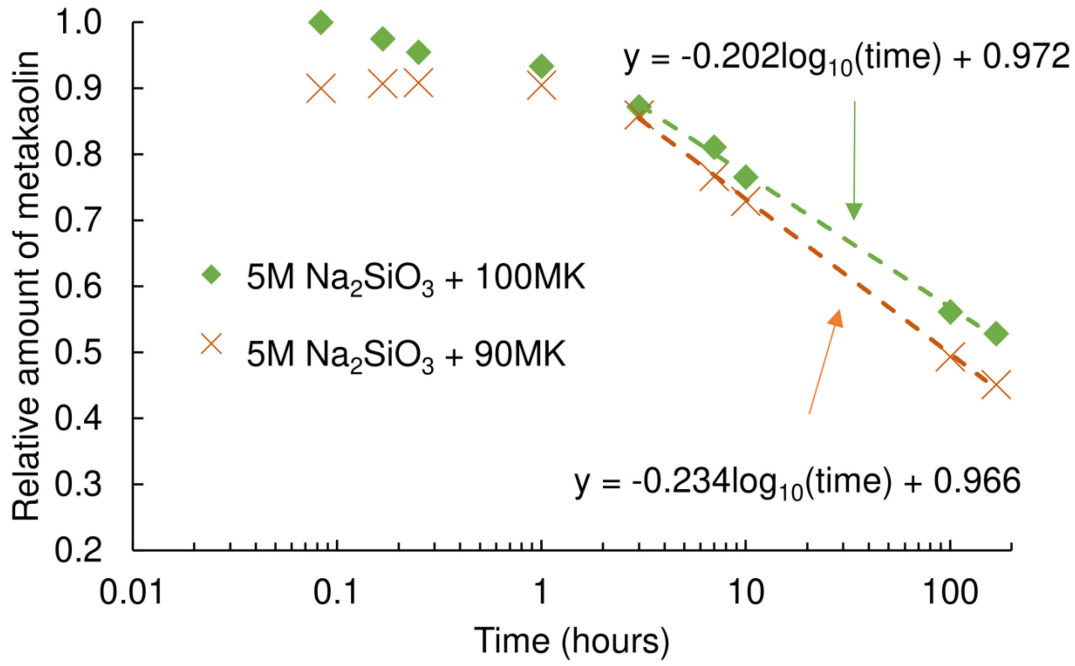

570

571 Figure 10. Relative amount of unreacted metakaolin in 5M Na_2SiO_3 + 100MK and 5M Na_2SiO_3 +
572 90MK as a function of reaction time, obtained from quantification of FTIR and XRD data. Data
573 points between 3 and 168 hours (7 days) have been fitted using a $\log_{10}$(time) function. Note that
574 the time axis is logarithmic.

575

576 The rate of metakaolin dissolution for the 10M Na_2SiO_3 pastes (100MK and 90MK) is shown in
577 Figure 11, where clear differences are seen in comparison with the 5M Na_2SiO_3 pastes (shown in
578 Figure 10). In contrast with the 5M samples where metakaolin dissolution occurs faster for the
579 90MK paste, it is the 100MK paste that undergoes more rapid metakaolin dissolution in the 10M
580 Na_2SiO_3 system (compared with the 90MK paste). This is most apparent via comparison of the
581 rate constants obtained in Figure 11 (-0.398 $hour^{-1}$ for 100MK and -0.109 $hour^{-1}$ for 90MK). This
582 finding for the 10M Na_2SiO_3 pastes disagrees with the results presented by Chen *et al.* where it

583 was reported that the addition of calcium hydroxide leads to a faster rate of metakaolin dissolution
584 and more extensive dissolution overall. However, there are clear differences between the Chen *et*
585 *al.* investigation and our work, specifically regarding the amount of calcium hydroxide used (~15
586 % by weight of metakaolin compared with 10 % in this investigation) as well as the silicate
587 modulus of the activating solution (2 for Chen *et al*. compared to 1 used in this investigation).
588 Furthermore, in this investigation the metakaolin amount was reduced to accommodate the
589 incorporation of calcium hydroxide (since calcium hydroxide is added as a powder) whereas for
590 Chen *et al.* the calcium hydroxide amount was in addition to the original amount of metakaolin. It
591 can be postulated that with a higher level of calcium addition, the dissolution of metakaolin will
592 proportionally increase. However, further investigation is necessary to investigate if this is the
593 case.

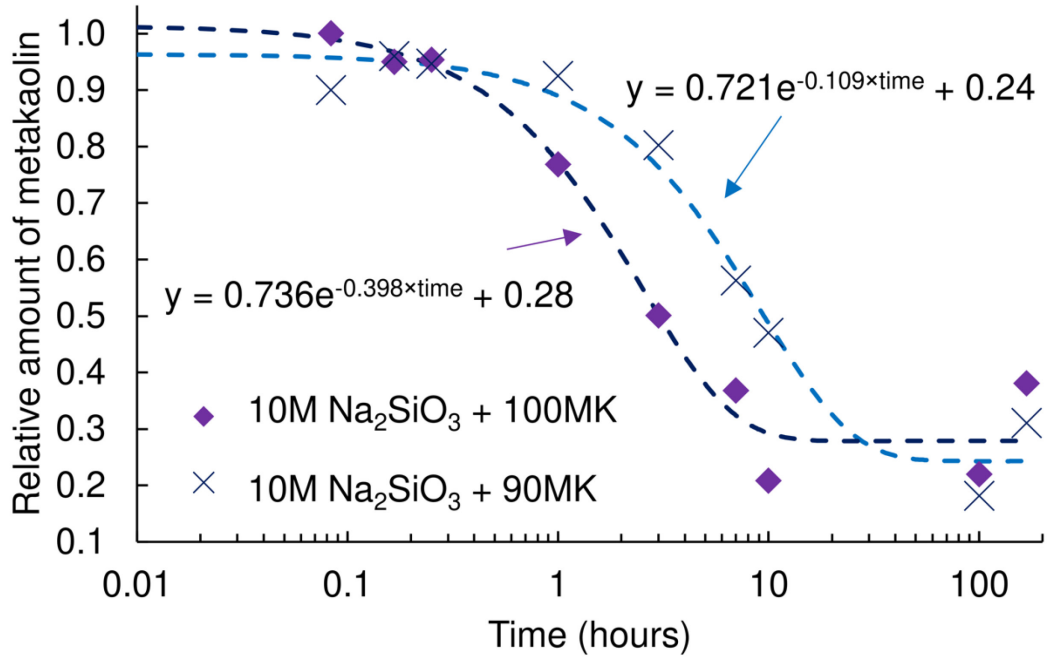

Figure 11. Relative amount of unreacted metakaolin in 10M Na_2SiO_3 + 100MK and 10M Na_2SiO_3 + 90MK as a function of reaction time, obtained from quantification of FTIR and XRD data. Data points have been fitted using a pseudo-first order rate expression. Note that the time axis is logarithmic.

Although it cannot be definitively stated from these data that the C-A-S-H gel is absent at later stages of reaction in the 5 and 10M Na_2SiO_3 + 90MK pastes, there is no evident shoulder intensity positioned near 920 cm^{-1} that systematically shifts to higher wavenumbers beyond 3 hours, which would be an indicator that the initial C-A-S-H gel gradually evolves into a calcium-containing N-A-S-H (N-(C)-A-S-H) gel after several hours of reaction. However, it is known that a synthetic C-A-S-H gel that mimics the final gel formed in alkali-activated slag gives rise to the Si-O-T peak at ~950 cm^{-1} [65], making it extremely difficult to ascertain from FTIR data if two gels co-exist at

607 later times (i.e., at 7 days) or if the initial C-A-S-H gel has been incorporated into a single N-(C)-
608 A-S-H gel.

609

610 Due to the evident delay of metakaolin dissolution seen in Figure 7 for the 5 and 10M NaOH +
611 90MK pastes compared with their 100MK counterparts in Figure 3, specifically by the more
612 prominent metakaolin peak at 10 hrs after mixing in the 90MK pastes, quantitative analysis of
613 unreacted metakaolin has not been carried out in this investigation. This delay is even more evident
614 in Figure 8, where the abrupt decrease in Si-O-T wavenumber occurs at later times for the 90MK
615 pastes compared with their 100MK counterparts. These results show that, without the presence of
616 soluble silica in the activator, the calcium hydroxide cannot cause enhanced metakaolin
617 dissolution. At the later stages of reaction, the type of gel growth is seen to be independent of the
618 presence of calcium hydroxide for the 5 and 10M NaOH pastes, as already mentioned in Section
619 3.3.2.

620

621

622 ***3.5 Role of Calcium Hydroxide in the Alkali-activation Reaction of Aluminosilicates***

623 This investigation shows that the efficacy of calcium hydroxide to accelerate the reaction kinetics
624 of alkali-activated metakaolin is reliant on the availability of soluble silica (or potentially another
625 soluble species) at the outset of the reaction. As alluded to in the literature [77], this silica is
626 necessary for the formation of a C-A-S-H gel during the early stages of reaction, which
627 subsequently instigates a chain of events starting with the increase of solution pH (via calcium
628 hydroxide dissolution), increased rate of metakaolin dissolution and associated increase of the rate

629 of N-A-S-(H) gel precipitation [34]. Our results show that this enhanced behavior occurs only in
630 the 5M Na_2SiO_3 + 90MK paste, and not its 10M equivalent. The statement that dissolution of
631 calcium hydroxide in the sodium silicate solution leads to an increase of solution pH is supported
632 by thermodynamic calculations that have been performed using GEMS software on the 5M
633 Na_2SiO_3 system. Thermodynamic modeling predicts that the 5M Na_2SiO_3 activator has an initial
634 pH of 13.8, and after addition of the calcium hydroxide (assuming no metakaolin dissolution) the
635 pH is seen to increase to 14.2 (along with the formation of C-S-H gel). The validity of the
636 calculation of the initial pH (13.8) is supported by experimental data obtained by Svensson et al.,
637 where a pH of 13.62 was measured for a ~4.3M Na_2SiO_3 solution [78]. Unfortunately,
638 thermodynamic modeling of the 10M Na_2SiO_3 activator failed to provide a pH value close to
639 experimental data (thermodynamic calculation predicted a pH of 13.4 for the 10M Na_2SiO_3
640 activator while experimental data for a ~8.8M equivalent solution was measured at a pH of 14.09).
641 Therefore, the impact of calcium hydroxide on the pH for the 10M Na_2SiO_3 activator is not
642 reported in this investigation. For 5 and 10M NaOH + 90MK this favorable chain of events does
643 not occur due to the absence of soluble silica at the beginning of the reaction, and, instead, the
644 calcium hydroxide remains inert due to the common ion effect.
645
646 In addition to the favorable influence of calcium hydroxide for increasing the reaction kinetics of
647 the 5M Na_2SiO_3-activated metakaolin system, it has been shown by Chen *et al.* that a calcium
648 hydroxide leads to a shortening of setting time [34]. However, the impact of calcium hydroxide on
649 compressive strength is still to be elucidated, particularly for the 5M paste (preliminary
650 unpublished results indicate some strength increase). It should be noted that mechanical strength
651 of a cementitious material is largely influenced by the water content of the paste [79,80], and

652 therefore the strength of alkali-activated metakaolin will be strongly dependent on the metakaolin
653 source (rotary kiln or flash calcination) and associated water demand (water-to-metakaolin wt.
654 ratio of 0.9 and <0.5, respectively).
655
656 ***3.6 Impact of calcium hydroxide on CO_2 emissions of AAM***
657 The use of calcium hydroxide may seem counterintuitive to the overall goal of sustainability that
658 is implicit to the design of alkali-activated materials. Specifically, calcium hydroxide is produced
659 by the decomposition of calcium carbonate (at ~800 °C, forming calcium oxide) followed by
660 hydration (i.e., exposure to water). Life-cycle assessment of calcium hydroxide manufacturing has
661 shown that 850 kg of CO_2 is generated per tonne of calcium hydroxide [81] (compared with 890
662 kg CO_2/tonne for OPC) [82]. The production of metakaolin creates ~300 kg CO_2 per tonne [83],
663 with additional CO_2 reductions if flash calcined metakaolin is sourced [82] (~200 kg CO_2 per
664 tonne). The main source of CO_2 emissions associated with alkali-activated materials is the alkalis,
665 since the manufacture of one tonne of sodium silicate solution (assuming 37 wt. % sodium silicate
666 solid) has a CO_2 equivalent of 400 kg [83]. Therefore, altering the precursor composition from
667 metakaolin (300 kg CO_2 per tonne [83]) to 90 wt. % metakaolin and 10 wt. % calcium hydroxide
668 (355 kg CO_2 per tonne [83]) leads to a slight increase in emissions (18%), but these are offset by
669 the significant reductions in alkali concentration (halving the alkali concentration from 10 to 5M
670 leads to a 50% reduction in emissions), making calcium hydroxide-containing alkali-activated
671 metakaolin a sustainable cement option (~70% lower CO_2 emissions compared with OPC/fly ash
672 paste).
673

4. Conclusions

In this study, the influence of calcium hydroxide on the formation mechanisms of alkali-activated metakaolin pastes was elucidated using Fourier transform infrared spectroscopy, X-ray diffraction and isothermal conduction calorimetry. It was found that calcium hydroxide minimally impacts NaOH-activated metakaolin systems, in contrast to the significant effects on Na_2SiO_3-activated metakaolin mixtures and particularly the 5M system. The common ion effect dominates the behavior in the NaOH-activated pastes, causing the added calcium hydroxide to remain relatively inert, leading to a reduced rate of metakaolin dissolution and a delay in N-A-S-(H) gel formation. In contrast, accelerated formation of N-A-S-(H) gel occurs when calcium hydroxide is added to 5M Na_2SiO_3-activated metakaolin, attributed to the initial formation of C-A-S-H gel that promotes metakaolin dissolution and subsequent N-A-S-(H) gel precipitation. Specifically, as calcium is incorporated into the C-A-S-H gel, an increase in overall pH in the 5M Na_2SiO_3 system due to calcium hydroxide dissolution encourages more rapid precursor dissolution. Overall, it is clear that the addition of calcium hydroxide to Na_2SiO_3-activated metakaolin is a promising approach for reducing activator concentration and warrants further investigation.

Supplementary Material

Supplementary Material is available. Full FTIR spectra at 7 days. FTIR false color plots from *in situ* measurements. FTIR spectra from *in situ* measurements before, during and after a sample lost contact with the ATR diamond.

Acknowledgments

This work was funded by the National Science Foundation, Grant No. 1727346.

References

[1] E. Gartner, Industrially interesting approaches to "low-CO_2" cements, Cem. Concr. Res. 34 (2004) 1489–1498. https://doi.org/10.1016/j.cemconres.2004.01.021.

[2] J.G.J. Olivier, G. Janssens-Maenhout, M. Muntean, J.A.H.W. Peters, Trends in global CO_2 emissions report, The Hague, Netherlands, 2016. https://doi.org/10.2788/33777.

[3] J.L. Provis, Alkali-activated materials, Cem. Concr. Res. 114 (2018) 40–48. https://doi.org/10.1016/j.cemconres.2017.02.009.

[4] J.L. Provis, J.S.J. van Deventer, Geopolymers - structure, processing, properties and industrial applications, Woodhead Publishing Limited, Boca Raton, 2009. https://doi.org/https://doi.org/10.1533/9781845696382.

[5] S. Alberici, J. De Beer, I. Van Der Hoorn, M. Staats, Fly ash and blast furnace slag for cement manufacturing, BEIS Res. Pap. No. 19. 35 (2017) 35. https://assets.publishing.service.gov.uk/government/uploads/system/uploads/attachment_data/file/660888/fly-ash-blast-furnace-slag-cement-manufacturing.pdf.

[6] T.L. Robl, C.J. McCormick, We are running out of fly ash: the nature of regional supply problems, in: DOE/FETC 3rd Conf. Unburned Carbon Util. Fly Ash, Pittsburgh, PA, 1997. http://cdnassets.hw.net/1b/2e/7fd837ed40f4be102b391632af40/robl.pdf (accessed November 14, 2018).

[7] S. Salvador, Pozzolanic properties of flash-calcined kaolinite: A comparative study with soak-calcined products, Cem. Concr. Res. 25 (1995) 102–112. https://doi.org/10.1016/0008-8846(94)00118-I.

[8] A. Palomo, F.P. Glasser, Chemically-bonded cementitious materials based on metakaolin, Br. Ceram. Trans. J. 91 (1992) 107–112.

[9] D.M. Flanagan, Mineral Commodity Summary: Clays, USGS. (2016) 50–51. https://minerals.usgs.gov/minerals/pubs/commodity/clays/mcs-2017-clays.pdf (accessed March 31, 2019).

[10] R.L. Virta, Clay and shale, in: U.S. Geol. Survery Miner. Yearb., 2003: pp. 18.1-18.26. https://minerals.usgs.gov/minerals/pubs/commodity/clays/claysmyb03.pdf (accessed February 17, 2019).

[11] G.W. Brindley, M. Nakahira, The kaolinite-mullite reaction series: II, metakaolin, J. Am. Ceram. Soc. 42 (1959) 314–318. https://doi.org/10.1111/j.1151-2916.1959.tb14315.x.

[12] K.J.D. MacKenzie, I.W.M. Brown, M.E. Bowden, R.H. Meinhold, Outstanding problems in the kaolinite-mullite reaction sequence investigated by 29Si and 27Al solid-state nuclear magnetic resonance: I, metakaolinite, J. Am. Ceram. Soc. 68 (1985) 293–297. https://doi.org/10.1111/j.1151-2916.1985.tb15229.

[13] C.E. White, J.L. Provis, T. Proffen, D.P. Riley, J.S.J. van Deventer, Combining density functional theory (DFT) and pair distribution function (PDF) analysis to solve the structure of metastable materials: the case of metakaolin, Phys. Chem. Chem. Phys. 12 (2010) 3239. https://doi.org/10.1039/b922993k.

[14] H. Rahier, B. Wullaert, B. Van Mele, Influence of the degree of dehydroxylation of kaolinite on the properties of aluminosilicate glasses, J. Therm. Anal. Calorim. 62 (2000) 417–427. https://doi.org/10.1023/A:1010138130395.

[15] C.E. White, J.L. Provis, T. Proffen, D.P. Riley, J.S.J. van Deventer, Density functional modeling of the local structure of kaolinite subjected to thermal dehydroxylation, J. Phys. Chem. A. 114 (2010) 4988–4996. https://doi.org/10.1021/jp911108d.

[16] J.L. Provis, S.A. Bernal, Geopolymers and related alkali-activated materials, Annu. Rev. Mater. Res. 44 (2014) 299–327. https://doi.org/10.1146/annurev-matsci-070813-113515.

[17] L. Chen, Z. Wang, Y. Wang, J. Feng, Preparation and properties of alkali activated metakaolin-based geopolymer, Materials (Basel). 9 (2016) 767. https://doi.org/10.3390/ma9090767.

[18] P. Duxson, J.L. Provis, Designing precursors for geopolymer cements, J. Am. Ceram. Soc. 91 (2008) 3864–3869. https://doi.org/10.1111/j.1551-2916.2008.02787.x.

[19] S. Alonso, A. Palomo, Calorimetric study of alkaline activation of calcium hydroxide–metakaolin solid mixtures, Cem. Concr. Res. 31 (2001) 25–30. https://doi.org/10.1016/S0008-8846(00)00435-X.

[20] K. Yang, C.E. White, Modeling the formation of alkali aluminosilicate gels at the mesoscale using coarse-grained Monte Carlo, Langmuir. 32 (2016) 11580–11590. https://doi.org/10.1021/acs.langmuir.6b02592.

[21] C.E. White, J.L. Provis, B. Bloomer, N.J. Henson, K. Page, In situ X-ray pair distribution function analysis of geopolymer gel nanostructure formation kinetics, Phys. Chem. Chem. Phys. 15 (2013) 8573. https://doi.org/10.1039/c3cp44342f.

[22] P. Duxson, G.C. Lukey, J.S.J. van Deventer, Physical evolution of Na-geopolymer derived from metakaolin up to 1000°C, J. Mater. Sci. 42 (2007) 3044–3054. https://doi.org/10.1007/s10853-006-0535-4.

[23] F. Wang, K. Kovler, J.L. Provis, A. Buchwald, M. Cyr, C. Patapy, S. Kamali-Bernard, L. Courard, K. Sideris, Metakaolin, in: Prop. Fresh Hardened Concr. Contain. Suppl. Cem. Mater., 2018: pp. 153–179. https://doi.org/10.1007/978-3-319-70606-1_5.

[24] M. Król, J. Minkiewicz, W. Mozgawa, IR spectroscopy studies of zeolites in geopolymeric

materials derived from kaolinite, J. Mol. Struct. 1126 (2016) 200–206. https://doi.org/10.1016/j.molstruc.2016.02.027.

[25] M. Criado, W. Aperador, I. Sobrados, Microstructural and mechanical properties of alkali activated Colombian raw materials, Materials (Basel). 9 (2016) 158. https://doi.org/10.3390/ma9030158.

[26] M.L. Granizo, S. Alonso, M.T. Blanco-Varela, A. Palomo, Alkaline activation of metakaolin effect of calcium hydroxide in the products of reaction, J. Am. Ceram. Soc. 31 (2002) 225–231. https://doi.org/10.1111/j.1151-2916.2002.tb00070.x.

[27] Z. Zhang, H. Wang, J.L. Provis, F. Bullen, A. Reid, Y. Zhu, Quantitative kinetic and structural analysis of geopolymers. Part 1. The activation of metakaolin with sodium hydroxide, Thermochim. Acta. 539 (2012) 23–33. https://doi.org/10.1016/j.tca.2012.03.021.

[28] C.E. White, K. Page, N.J. Henson, J.L. Provis, In situ synchrotron X-ray pair distribution function analysis of the early stages of gel formation in metakaolin-based geopolymers, Appl. Clay Sci. 73 (2013) 17–25. https://doi.org/10.1016/j.clay.2012.09.009.

[29] A. Buchwald, H. Hilbig, C. Kaps, Alkali-activated metakaolin-slag blends—performance and structure in dependence of their composition, J. Mater. Sci. 42 (2007) 3024–3032. https://doi.org/10.1007/s10853-006-0525-6.

[30] R. Si, S. Guo, Q. Dai, Influence of calcium content on the atomic structure and phase formation of alkali-activated cement binder, J. Am. Ceram. Soc. 102 (2019) 1479–1494. https://doi.org/10.1111/jace.15968.

[31] S. Alonso, A. Palomo, Alkaline activation of metakaolin and calcium hydroxide mixtures: influence of temperature, activator concentration and solids ratio, Mater. Lett. 47 (2001) 55–62. https://doi.org/10.1016/S0167-577X(00)00212-3.

[32] C.K. Yip, J.S.J. Van Deventer, Microanalysis of calcium silicate hydrate gel formed within a geopolymeric binder, J. Mater. Sci. 38 (2003) 3851–3860. https://doi.org/10.1023/A:1025904905176.

[33] C.K. Yip, G.C. Lukey, J.S.J. van Deventer, The coexistence of geopolymeric gel and calcium silicate hydrate at the early stage of alkaline activation, Cem. Concr. Res. 35 (2005) 1688–1697. https://doi.org/10.1016/j.cemconres.2004.10.042.

[34] X. Chen, A. Sutrisno, L.J. Struble, Effects of calcium on setting mechanism of metakaolin-based geopolymer, J. Am. Ceram. Soc. 101 (2018) 957–968. https://doi.org/10.1111/jace.15249.

[35] P.S. de Silva, F.P. Glasser, Hydration of cements based on metakaolin: thermochemistry, Adv. Cem. Res. 3 (1990) 167–177. https://doi.org/10.1680/adcr.1990.3.12.167.

[36] S.A. Bernal, J.L. Provis, V. Rose, R. Mejía de Gutierrez, Evolution of binder structure in sodium silicate-activated slag-metakaolin blends, Cem. Concr. Compos. 33 (2011) 46–54. https://doi.org/10.1016/j.cemconcomp.2010.09.004.

[37] S.A. Bernal, E.D. Rodríguez, R. Mejía de Gutiérrez, M. Gordillo, J.L. Provis, Mechanical

and thermal characterisation of geopolymers based on silicate-activated metakaolin/slag blends, J. Mater. Sci. 46 (2011) 5477–5486. https://doi.org/10.1007/s10853-011-5490-z.

[38] K. Dombrowski, A. Buchwald, M. Weil, The influence of calcium content on the structure and thermal performance of fly ash based geopolymers, J. Mater. Sci. 42 (2007) 3033–3043. https://doi.org/10.1007/s10853-006-0532-7.

[39] J. Temuujin, A. van Riessen, R. Williams, Influence of calcium compounds on the mechanical properties of fly ash geopolymer pastes, J. Hazard. Mater. 167 (2009) 82–88. https://doi.org/10.1016/j.jhazmat.2008.12.121.

[40] R. Salimi, J. Vaughan, Crystallisation of tricalcium aluminate from sodium aluminate solution using slaked lime, Powder Technol. 294 (2016) 472–483. https://doi.org/10.1016/j.powtec.2016.03.017.

[41] B.I. Whittington, C.M. Cardile, The chemistry of tricalcium aluminate hexahydrate relating to the Bayer industry, Int. J. Miner. Process. 48 (1996) 21–38. https://doi.org/10.1016/S0301-7516(96)00011-7.

[42] A. Buchwald, H.-D. Zellmann, C. Kaps, Condensation of aluminosilicate gels—model system for geopolymer binders, J. Non. Cryst. Solids. 357 (2011) 1376–1382. https://doi.org/10.1016/j.jnoncrysol.2010.12.036.

[43] K. Gong, Y. Cheng, L.L. Daemen, C.E. White, In situ quasi-elastic neutron scattering study on the water dynamics and reaction mechanisms in alkali-activated slags, Phys. Chem. Chem. Phys. 21 (2019) 10277–10292. https://doi.org/10.1039/C9CP00889F.

[44] A. Fernández-Jiménez, F. Puertas, Setting of alkali-activated slag cement. Influence of activator nature, Adv. Cem. Res. 13 (2001) 115–121. https://doi.org/10.1680/adcr.2001.13.3.115.

[45] A. Fernández-Jiménez, F. Puertas, Effect of activator mix on the hydration and strength behaviour of alkali-activated slag cements, Adv. Cem. Res. 15 (2003) 129–136. https://doi.org/10.1680/adcr.2003.15.3.129.

[46] S.A. Bernal, J.L. Provis, R.J. Myers, R. San Nicolas, J.S.J. van Deventer, Role of carbonates in the chemical evolution of sodium carbonate-activated slag binders, Mater. Struct. 48 (2015) 517–529. https://doi.org/10.1617/s11527-014-0412-6.

[47] N. Mobasher, S.A. Bernal, J.L. Provis, Structural evolution of an alkali sulfate activated slag cement, J. Nucl. Mater. 468 (2016) 97–104. https://doi.org/10.1016/j.jnucmat.2015.11.016.

[48] N. Garg, C.E. White, Mechanism of zinc oxide retardation in alkali-activated materials: an in situ X-ray pair distribution function investigation, J. Mater. Chem. A. 5 (2017) 11794–11804. https://doi.org/10.1039/C7TA00412E.

[49] A. Autef, E. Joussein, G. Gasgnier, S. Rossignol, Importance of metakaolin impurities for geopolymer based synthesis, in: Dev. Strateg. Mater. a Collect. Pap., 2013: pp. 1–12. https://doi.org/10.1002/9781118807743.ch1.

[50] S. Boonjaeng, P. Chindaprasirt, K. Pimraksa, Lime-calcined clay materials with alkaline

activation: Phase development and reaction transition zone, Appl. Clay Sci. 95 (2014) 357–364. https://doi.org/10.1016/j.clay.2014.05.002.

[51] J. Rocha, J. Klinowski, Solid-state NMR studies of the structure and reactivity of metakaolinite, Angew. Chemie Int. Ed. English. 29 (1990) 553–554. https://doi.org/10.1002/anie.199005531.

[52] P. Duxson, J.L. Provis, G.C. Lukey, F. Separovic, J.S.J. van Deventer, ^{29}Si NMR study of structural ordering in aluminosilicate geopolymer gels, Langmuir. 21 (2005) 3028–3036. https://doi.org/10.1021/la047336x.

[53] P. Duxson, G.C. Lukey, J.S.J. van Deventer, Evolution of gel structure during thermal processing of Na-geopolymer gels, Langmuir. 22 (2006) 8750–8757. https://doi.org/10.1021/la0604026.

[54] B. Walkley, R. San Nicolas, M.-A. Sani, G.J. Rees, J. V Hanna, J.S.J. van Deventer, J.L. Provis, Phase evolution of C-(N)-A-S-H/N-A-S-H gel blends investigated via alkali-activation of synthetic calcium aluminosilicate precursors, Cem. Concr. Res. 89 (2016) 120–135. https://doi.org/10.1016/j.cemconres.2016.08.010.

[55] I. Lancellotti, M. Catauro, C. Ponzoni, F. Bollino, C. Leonelli, Inorganic polymers from alkali activation of metakaolin: Effect of setting and curing on structure, J. Solid State Chem. 200 (2013) 341–348. https://doi.org/10.1016/j.jssc.2013.02.003.

[56] O. Burciaga-Díaz, J.I. Escalante-García, R.X. Magallanes-Rivera, Compressive strength and microstructural evolution of metakaolin geopolymers exposed at high temperature, ALCONPAT J. 5 (2015) 52–66.

[57] J.J. Thomas, A new approach to modeling the nucleation and growth kinetics of tricalcium silicate hydration, J. Am. Ceram. Soc. 90 (2007) 3282–3288. https://doi.org/10.1111/j.1551-2916.2007.01858.x.

[58] R. Alizadeh, L. Raki, J.M. Makar, J.J. Beaudoin, I. Moudrakovski, Hydration of tricalcium silicate in the presence of synthetic calcium–silicate–hydrate, J. Mater. Chem. 19 (2009) 7937. https://doi.org/10.1039/b910216g.

[59] J.L. Provis, Modelling the formation of geopolymers, The University of Melbourne, 2006.

[60] L. Vidal, E. Joussein, M. Colas, J. Cornette, J. Sanz, I. Sobrados, J. Gelet, J. Absi, S. Rossignol, Controlling the reactivity of silicate solutions: A FTIR, Raman and NMR study, Colloids Surfaces A Physicochem. Eng. Asp. 503 (2016) 101–109. https://doi.org/10.1016/j.colsurfa.2016.05.039.

[61] H. Jansson, D. Bernin, K. Ramser, Silicate species of water glass and insights for alkali-activated green cement, AIP Adv. 5 (2015) 067167. https://doi.org/10.1063/1.4923371.

[62] P. Steins, A. Poulesquen, O. Diat, F. Frizon, Structural evolution during geopolymerization from an early age to consolidated material, Langmuir. 28 (2012) 8502–8510. https://doi.org/10.1021/la300868v.

[63] P. De Silva, F. Glasser, Pozzolanic activation of metakaolin, Adv. Cem. Res. 4 (1992) 167–78. https://doi.org/10.1680/adcr.1992.4.16.167.

[64] A. Gameiro, A. Santos Silva, R. Veiga, A. Velosa, Hydration products of lime–metakaolin pastes at ambient temperature with ageing, Thermochim. Acta. 535 (2012) 36–41. https://doi.org/10.1016/j.tca.2012.02.013.

[65] E. Kapeluszna, Ł. Kotwica, A. Różycka, Ł. Gołek, Incorporation of Al in C-A-S-H gels with various Ca/Si and Al/Si ratio: Microstructural and structural characteristics with DTA/TG, XRD, FTIR and TEM analysis, Constr. Build. Mater. 155 (2017) 643–653. https://doi.org/10.1016/j.conbuildmat.2017.08.091.

[66] I. García-Lodeiro, A. Palomo, A. Fernández-Jiménez, D.E. Macphee, Compatibility studies between N-A-S-H and C-A-S-H gels. Study in the ternary diagram Na_2O–CaO–Al_2O_3–SiO_2–H_2O, Cem. Concr. Res. 41 (2011) 923–931. https://doi.org/10.1016/j.cemconres.2011.05.006.

[67] K. Gong, C.E. White, Nanoscale chemical degradation mechanisms of sulfate attack in alkali-activated slag, J. Phys. Chem. C. 122 (2018) 5992–6004. https://doi.org/10.1021/acs.jpcc.7b11270.

[68] R.J. Myers, B. Lothenbach, S.A. Bernal, J.L. Provis, Thermodynamic modelling of alkali-activated slag cements, Appl. Geochemistry. 61 (2015) 233–247. https://doi.org/10.1016/j.apgeochem.2015.06.006.

[69] Y. Xiong, A thermodynamic model for silica and aluminum in alkaline solutions with high ionic strength at elevated temperatures up to 100°C: Applications to zeolites, Am. Mineral. 98 (2013) 141–153. https://doi.org/10.2138/am.2013.4089.

[70] N. Garg, V.O. Özçelik, J. Skibsted, C.E. White, Nanoscale ordering and depolymerization of calcium silicate hydrates in the presence of alkalis, J. Phys. Chem. C. 123 (2019) 24873–24883. https://doi.org/10.1021/acs.jpcc.9b06412.

[71] R.J. Myers, S.A. Bernal, J.D. Gehman, J.S.J. van Deventer, J.L. Provis, The role of Al in cross-linking of alkali-activated slag cements, J. Am. Ceram. Soc. 98 (2015) 996–1004. https://doi.org/10.1111/jace.13360.

[72] I. García-Lodeiro, A. Fernández-Jiménez, A. Palomo, D.E. Macphee, Effect of calcium additions on N-A-S-H cementitious gels, J. Am. Ceram. Soc. 93 (2010) 1934–1940. https://doi.org/10.1111/j.1551-2916.2010.03668.x.

[73] P. Yu, R.J. Kirkpatrick, B. Poe, P.F. McMillan, X. Cong, Structure of calcium silicate hydrate (C-S-H): Near-, mid-, and far-infrared spectroscopy, J. Am. Ceram. Soc. 82 (2004) 742–748. https://doi.org/10.1111/j.1151-2916.1999.tb01826.x.

[74] S. Takahashi, D.R. Neuville, H. Takebe, Thermal properties, density and structure of percalcic and peraluminus CaO–Al_2O_3–SiO_2 glasses, J. Non. Cryst. Solids. 411 (2015) 5–12. https://doi.org/10.1016/j.jnoncrysol.2014.12.019.

[75] M. Wojdyr, Fityk: A general-purpose peak fitting program, J. Appl. Crystallogr. 43 (2010) 1126–1128. https://doi.org/10.1107/S0021889810030499.

[76] R.P. Williams, R.D. Hart, A. Van Riessen, Quantification of the extent of reaction of metakaolin-based geopolymers using X-ray diffraction, scanning electron microscopy, and energy-dispersive spectroscopy, J. Am. Ceram. Soc. 94 (2011) 2663–2670.

https://doi.org/10.1111/j.1551-2916.2011.04410.x.

[77] H.M. Khater, Effect of calcium on geopolymerization of aluminosilicate wastes, J. Mater. Civ. Eng. 24 (2012) 92–101. https://doi.org/10.1061/(ASCE)MT.1943-5533.0000352.

[78] I.L. Svensson, S. Sjöberg, L.O. Öhman, Polysilicate equilibria in concentrated sodium silicate solutions, J. Chem. Soc. Faraday Trans. 1. 82 (1986) 3635–3646. https://doi.org/10.1039/F19868203635.

[79] M. Lizcano, A. Gonzalez, S. Basu, K. Lozano, M. Radovic, Effects of water content and chemical composition on structural properties of alkaline activated metakaolin-based geopolymers, J. Am. Ceram. Soc. 95 (2012) 2169–2177. https://doi.org/10.1111/j.1551-2916.2012.05184.x.

[80] Z. Zuhua, Y. Xiao, H. Z, C. Yue, Role of water in the synthesis of calcined kaolin-based geopolymer, Appl. Clay Sci. 43 (2009) 218–223. https://doi.org/10.1016/j.clay.2008.09.003.

[81] U.E.P.A. Office of Air and Radiation, Technical support document for the lime manufacturing sector: Proposed rule for mandatory reporting of greenhouse gases, U.S. Environ. Prot. Agency. (2009). https://www.epa.gov/sites/production/files/2015-07/documents/subpartstsd.pdf.

[82] Y. Cancio Díaz, S. Sánchez Berriel, U. Heierli, A.R. Favier, I.R. Sánchez Machado, K.L. Scrivener, J.F. Martirena Hernández, G. Habert, Limestone calcined clay cement as a low-carbon solution to meet expanding cement demand in emerging economies, Dev. Eng. 2 (2017) 82–91. https://doi.org/10.1016/j.deveng.2017.06.001.

[83] G. Habert, C. Ouellet-Plamondon, Recent update on the environmental impact of geopolymers, RILEM Tech. Lett. 1 (2016) 17. https://doi.org/10.21809/rilemtechlett.2016.6.